



Upstream migration of avulsion sites on lowland deltas with river-mouth retreat



Jianguang Li^{a,b,*}, Vamsi Ganti^{c,d,**}, Chenglong Li^b, Hao Wei^b

^a Key Laboratory of Tectonics and Petroleum Resources (China University of Geosciences), Ministry of Education, Wuhan 430074, China

^b Key Laboratory of Theory and Technology of Petroleum Exploration and Development in Hubei Province, Wuhan 430074, China

^c Department of Geography, University of California Santa Barbara, Santa Barbara, CA, USA

^d Department of Earth Science, University of California Santa Barbara, Santa Barbara, CA, USA

ARTICLE INFO

Article history:

Received 13 March 2021

Received in revised form 21 September 2021

Accepted 25 October 2021

Available online 8 November 2021

Editor: J.-P. Avouac

Dataset link: <https://earthexplorer.usgs.gov/>

Dataset link:

<https://global-surface-water.appspot.com/>

Keywords:

backwater

avulsions

sea-level rise

coastal flooding

ABSTRACT

River deltas are fertile, populous landscapes that grow through river avulsions—episodic channel-jumping events. Historically, avulsions on deltas occurred at persistent locations, causing some of the deadliest recorded floods. Climate change and human activities are threatening to drown deltas but it is unknown how avulsions will respond because they occur infrequently on large, lowland deltas. Here, we use a low-gradient river delta formed on the margin of a lake in the Qaidam Basin, China, as a natural laboratory to explore how lowland deltas will respond to river-mouth retreat from accelerated relative sea-level rise. Using satellite imagery from 1973 to 2010 C.E., we identified and analyzed the response of 6 lobe-scale avulsions on the Sulengguole River delta to the seasonal expansion of the North Huoluxun Lake in the Qaidam Basin. We show that the seasonal lake-water area increase caused punctuated river-mouth retreat. In response, avulsion sites migrated upstream at a commensurate rate such that the avulsion length—streamwise distance of avulsion site to the river mouth—remained consistent and scaled with the backwater lengthscale, similar to large, lowland deltas. Results indicate that the drowning of lowland deltas from accelerated relative sea-level rise will shift avulsion hazards tens-to-hundreds of kilometers upstream, exposing new upstream communities to the risk of catastrophic flooding.

© 2021 The Authors. Published by Elsevier B.V. This is an open access article under the CC BY license (<http://creativecommons.org/licenses/by/4.0/>).

1. Introduction

River deltas are dynamic depositional landscapes that host bio-diverse ecosystems, fertile farmlands and approximately 339 million people worldwide (Edmonds et al., 2020; Giosan et al., 2014; Syvitski et al., 2009; Vörösmarty et al., 2009). They are extremely low-lying areas that are sustained by the intricate balance between fluvial sediment supply, sea level rise, and land subsidence. Climate change and human activities are, however, accelerating sea level rise and land compaction rates (Erban et al., 2014; Higgins et al., 2013; Levermann et al., 2013; Meehl et al., 2005; Nicholls and Cazenave, 2010), and diminishing fluvial sediment supply (Best and Darby, 2020; Syvitski et al., 2005; Vörösmarty et al., 2003)—changes that are drowning many river deltas world-

wide (e.g., Blum and Roberts, 2009; Edmonds et al., 2020; Giosan et al., 2014; Syvitski et al., 2009; Vörösmarty et al., 2009). In addition, coastal flooding can cause wetland loss and river mouth retreat (Nicholls, 2004; Nicholls and Cazenave, 2010; Syvitski, 2008), which can be accentuated by tropical cyclones (Wang and Toumi, 2021) and accelerated sea-level rise (Woodruff et al., 2013). We need a mechanistic understanding of how river deltas will respond to river-mouth retreat from accelerated relative sea-level rise (combination of sea level rise and land subsidence) and coastal inundation to assess future flood risk and inform policy decisions about sustainable management of river deltas.

At the largest scale, river deltas grow through episodic channel-jumping events, called river avulsions (Mohrig et al., 2000; Slingerland and Smith, 2004), where an abrupt shift in the river course leads to the nourishment of new parts of the deltaic plain with sediment (Jerolmack, 2009) (Fig. 1A). Avulsions shift the locus of sedimentation on deltas and lead to the construction of new delta lobes (Jerolmack, 2009) (Fig. 1A). While avulsions can help combat land loss (Kim et al., 2009), they are also a significant short-term hazard that led to some of the deadliest historical floods (Kid-

* Corresponding author at: Key Laboratory of Tectonics and Petroleum Resources (China University of Geosciences), Ministry of Education, Wuhan 430074, China.

** Corresponding author at: Department of Geography, University of California Santa Barbara, Santa Barbara, CA, USA.

E-mail addresses: jianguangli@cug.edu.cn (J. Li), vganti@ucsb.edu (V. Ganti).

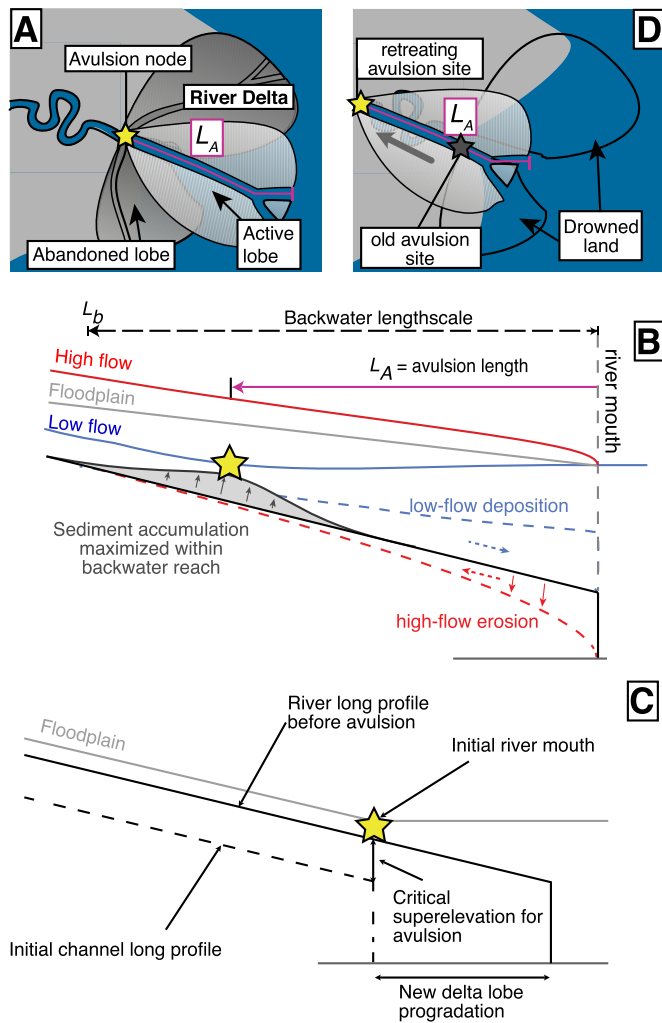


Fig. 1. Backwater and geometric hypotheses for lobe-scale avulsions on deltas. (A) Schematic planform of a river delta constructed through repeated cycles of lobe-scale avulsions that occur at a consistent distance upstream of the river mouth (L_A). (B) Schematic longitudinal profile view showing how the natural flood discharge variability and nonuniform flows within the backwater zone lead to the preferential location for avulsions (yellow star), i.e., the backwater hypothesis. Low flows (blue line) cause a depositional wave to propagate downstream (dashed blue line) within the backwater zone, and floods (red line) cause an erosional wave to propagate upstream from the river mouth (dashed red line). The imbalance between these zones of erosion and deposition lead to sediment accumulation and preferential avulsions within the backwater zone (Chadwick et al., 2019; Chatanantavet et al., 2012; Ganti et al., 2016a). (C) Under the geometric hypothesis, the avulsion length scales with the typical progradation length during an interavulsion period, which scales with the backwater lengthscale. Delta-lobe progradation causes riverbed aggradation and the disconnect between the rates of sedimentation within the channel and the floodplain causes avulsion sites to be associated with a slope-break in distal floodplain profiles (Ratliff et al., 2021). (D) Accelerated relative sea-level rise and storm surges will cause the drowning of coastal areas and the upstream retreat of the river mouth. Under the backwater and geometric hypotheses, the avulsion location is tied to the river mouth and should translate upstream in concert with the river mouth (gray star to yellow star) such that the avulsion length remains constant. (For interpretation of the colors in the figures, the reader is referred to the web version of this article.)

der and Liu, 2017; Slingerland and Smith, 2004). Avulsions are a consequence of preferential riverbed aggradation that causes the river to become unstable and perched above its surrounding floodplain (Ganti et al., 2016b; Jerolmack and Mohrig, 2007; Mohrig et al., 2000). Historical avulsions on lowland deltas have occurred at a persistent location within the backwater zone of coastal rivers (Chatanantavet et al., 2012; Ganti et al., 2014; Jerolmack and Swenson, 2007) (Figs. 1A, 1B): the lowermost part of alluvial rivers

characterized by nonuniform flows caused by the effect of a constant water-surface elevation at the river mouth (Lamb et al., 2012) (Fig. 1B). The upstream extent of the nonuniform flows can span a few hundred meters to hundreds of kilometers based on the size of the river, and is approximated by the backwater lengthscale, $\bar{L}_b = h_c/S$, where h_c and S are the bankfull flow depth and the riverbed slope within the normal flow reach, respectively (Paola and Mohrig, 1996).

Theory and physical experiments indicate that the preferential avulsion site on deltas emerges because of the morphodynamic feedbacks within the backwater zone caused by the natural flood discharge variability (Chadwick et al., 2019; Chatanantavet et al., 2012; Ganti et al., 2016a) (Fig. 1B). Low flows cause flow deceleration and a wave of sedimentation that propagates downstream through the backwater zone; however, large floods are accompanied by flow acceleration through the backwater zone and the upstream propagation of an erosional wave from the river mouth (Chatanantavet and Lamb, 2014; Lamb et al., 2012) (Fig. 1B). Over multiple floods, the spatial imbalance between the regions of erosion and deposition causes a peak in sediment accumulation within the backwater zone that leads to avulsions (Chadwick et al., 2019; Chatanantavet et al., 2012; Ganti et al., 2016a, 2016b) (Fig. 1B). Field observations support the backwater hypothesis for avulsions on deltas with the avulsion length—streamwise distance of the avulsion site to the river mouth—ranging from $0.2\bar{L}_b$ to $1.3\bar{L}_b$ on large, lowland deltas (Chadwick et al., 2019; Chatanantavet et al., 2012; Ganti et al., 2019, 2016a; Jerolmack, 2009; Moodie et al., 2019).

Recent numerical models also indicate that the backwater scaling of avulsion sites can emerge from purely geometric considerations, even in the absence of natural flood-discharge variability (Chadwick et al., 2019; Ratliff et al., 2021). Under this geometric hypothesis, the critical amount of sedimentation needed to trigger an avulsion, which scales with h_c (Mohrig et al., 2000), is achieved when a delta-lobe progrades by a distance that scales with the backwater lengthscale, leading to the correlation between the avulsion length and the backwater lengthscale (Fig. 1C) (Chadwick et al., 2019; Ratliff et al., 2021). In this scenario, the preferential avulsion location arises from the differential rates of sedimentation in the channel and the surrounding floodplains, and avulsion sites coincide with an abrupt topographic slope-break in the distal floodplain profiles (Fig. 1C) (Ratliff et al., 2021).

The backwater and geometric hypotheses have important untested predictions for how avulsion sites on deltas will respond to river-mouth retreat (Chadwick et al., 2020; Ratliff et al., 2021). The landward retreat of the river mouth is expected to cause a commensurate shift in the backwater zone, and river-mouth retreat should be accompanied by a predictable landward migration of avulsion sites (Chadwick et al., 2020; Ganti et al., 2016a; Ratliff et al., 2021) (Fig. 1D). This theoretical prediction is yet to be tested because avulsions reoccur on centennial to millennial timescales on most large, lowland deltas (Ganti et al., 2014; Jerolmack and Mohrig, 2007), limiting the observations of natural avulsions. Consequently, it is uncertain how historical avulsion sites will change on river deltas in response to relative sea-level rise.

Deltas formed near inland lakes provide a natural laboratory to test the key prediction of how avulsion hazards will respond to river-mouth retreat. Climate change and human impacts are already altering the extent of global lakes (Adrian et al., 2009; Ma et al., 2010; Woolway et al., 2020), mimicking the effect that coastal inundation and accelerated sea-level rise will have on large, lowland deltas. Here, we combined time series analysis of satellite imagery, spaceborne digital elevation models, and field measurements of river morphometry to identify and analyze the response of lobe-scale avulsions on a low-gradient river draining into a lake

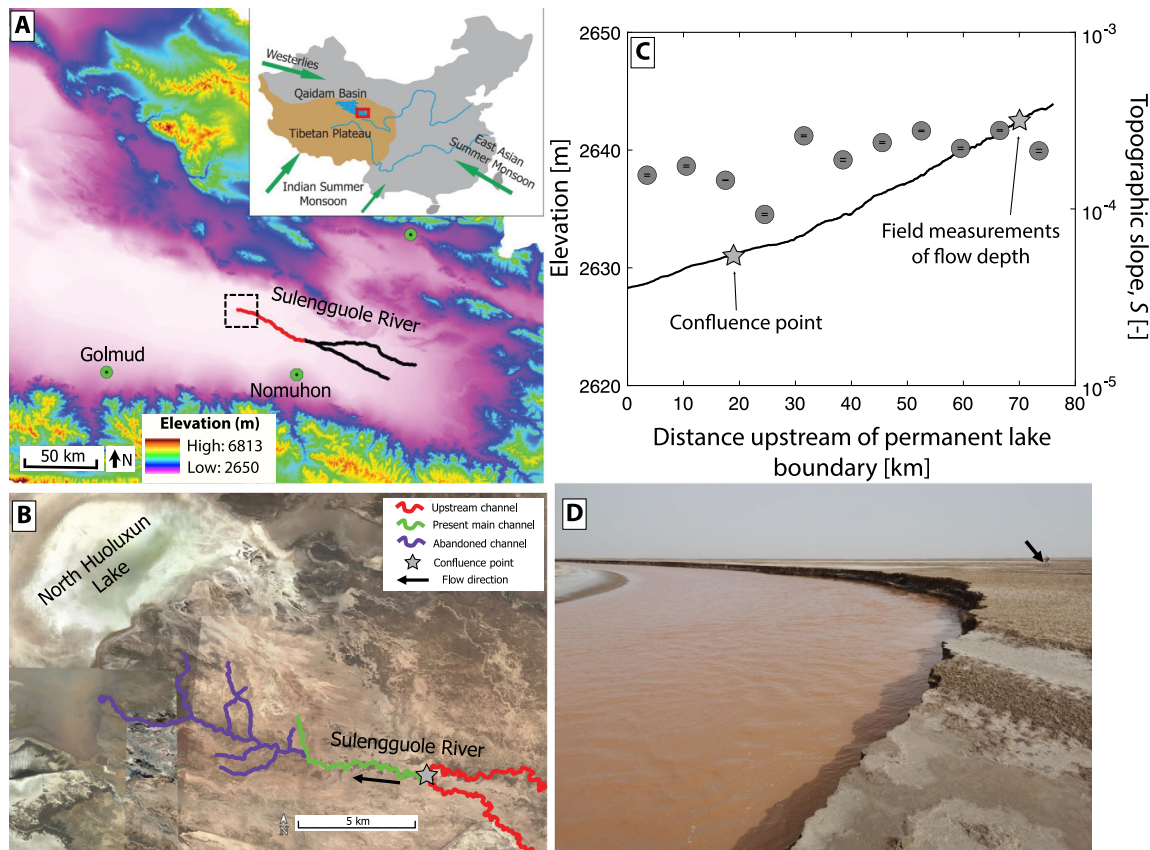


Fig. 2. Study area. (A) Shaded relief map of the east Qaidam Basin highlighting the location of the Sulengguole River. The inset figure shows the location of the basin. The red line along the Sulengguole River shows the extent of the longitudinal profile in panel C. Dashed rectangle indicates the spatial extent of panel B. (B) Google Earth Pro image (copyright Maxar Technologies) of distal Sulengguole River where two tributaries (red lines) join to form the present main channel (green line). The gray asterisk indicates the fixed reference point used for quantifying the river mouth and avulsion site retreat rates. The purple lines indicate the abandoned portions of the Sulengguole River. (C) The longitudinal profile along Sulengguole River derived from the TDX-12 m data. The profile is down the right tributary (looking downstream) towards the most distal portion of the abandoned channel (purple circle). The gray asterisks indicate the location of the reference point and the location of field surveys. (D) Field photograph of the Sulengguole River taken in late April 2019, roughly 70 km upstream of the lake boundary. Black arrow indicates person for scale.

in the Qaidam Basin, China, to river-mouth retreat caused by the expansion of the lake area.

2. Study area: Sulengguole River, Qaidam Basin, China

We focused on the lower reach of the Sulengguole River, which drains into the North Huoluxun Lake in the Qaidam Basin, China (Fig. 2). The Qaidam Basin is an internally drained basin at the northeastern margin of the Qinghai-Tibetan Plateau (Fig. 2A). The Qaidam basin has three major lakes: the Huoluxun, the Tajjinaer and the Dabuxun Lakes. Reduction in the areal extent of glaciers, human activities, and precipitation changes have caused substantial variations in the extent of the lakes in the Qaidam Basin over the last five decades (Duan, 2018; Li et al., 2019). Owing to the hyper-arid climate, the lake areas also show seasonal variations (Figs. 3, 4), where extreme precipitation and snowmelt is accompanied by the seasonal flooding of the low-lying areas surrounding the lakes. The Sulengguole River is a low-gradient, single-threaded perennial river in the Qaidam Basin (Figs. 2, S1)—fed by seepage water in the piedmont area—that drains into the North Huoluxun Lake in the southeast part of the basin (Fig. 2A). The North Huoluxun Lake was a permanent lake before an upstream dam construction in 2010 C.E., which gradually dried the lake. The dam construction led to the river running dry in the distal part after 2010 C.E. (Figs. S2). Before this time, the Sulengguole River delta experienced multiple cycles of natural lobe-scale avulsions, which are the focus of our study.

3. Methods

3.1. Identification and quantification of lobe-scale avulsions

We tracked the planform evolution of the distal Sulengguole River from 1973 C.E. to 2010 C.E. using Landsat multispectral imagery, including Landsat 1-5 MSS and Landsat 4-5 TM data (Fig. 3, Supplementary Movie S1). Detailed analysis could only be made from 1986 C.E. with the Landsat TM data because Landsat MSS sensor had a coarse spatial resolution. We defined an avulsion as a permanent change (abrupt or gradual) in the river course, and located the avulsion site using a combination of visual interpretation of the time series of Landsat imagery and water masks derived using a Modified Normalized Difference Water Index (MNDWI) (Figs. 3, S3). The MNDWI is widely used to extract water bodies due to stronger absorption by water of solar radiation in short-wave infrared bands than in near infrared and visible bands (Xu, 2006) (Figs. S1 to S3). MNDWI is computed as:

$$MNDWI = \frac{\rho_{green} - \rho_{SWIR}}{\rho_{green} + \rho_{SWIR}} \quad (1)$$

where for Landsat TM data, ρ_{green} is reflectance in Band 2 and ρ_{SWIR} is reflectance in Band 5. MNDWI mapping results in an image with values between 1 and -1, whereby pixels with high inundation probability have a high (positive) MNDWI. These time-series images were employed to generate water maps using the method of Otsu (1979), where single pixels were classified as wa-

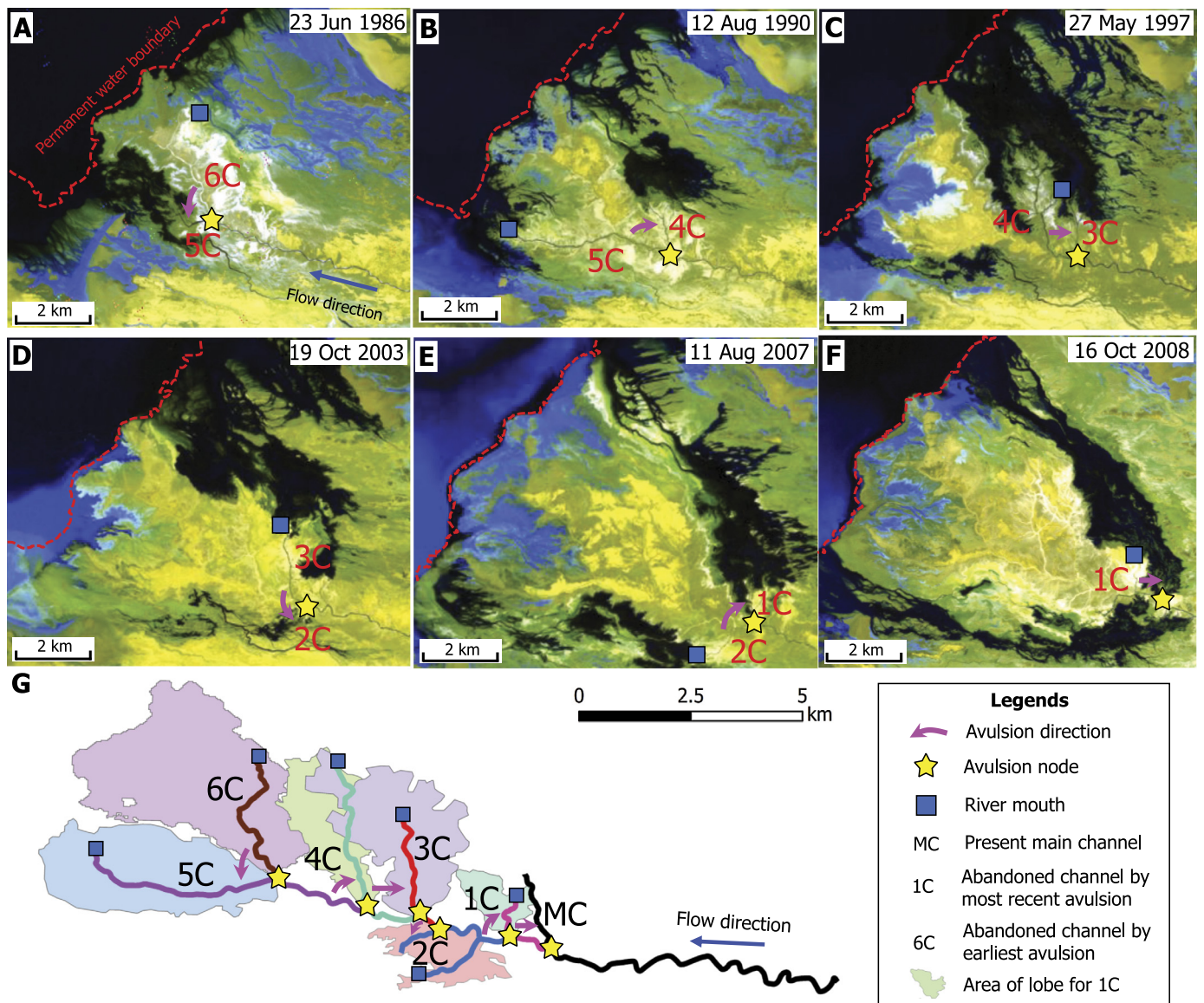


Fig. 3. Lobe-scale avulsions on the Sulengguole River. (A–F) Sequential satellite images that capture the lobe-scale avulsions on the Sulengguole River. The avulsion site and the river mouth of the parent channel are indicated by a yellow asterisk and blue square, respectively. Dashed red line indicates the boundary of the permanent lake waters. All satellite imagery are false-color composites with red (Band 7), green (Band 5) and blue (Band 1). (G) Reconstructed temporal history of lobe-scale avulsions on the Sulengguole River along with a visualization of the deltaic lobes (shaded colored area). The oldest abandoned channel is labeled 6C and 1C is the river channel abandoned by the latest avulsion in 2008 C.E.

ter if the computed MNDWI was greater than a dynamic threshold value. Overall, these water maps allowed for the identification of the abrupt changes in river course through time and aided the visual interpretation of time series of satellite images (Fig. S3). High-resolution satellite imagery on Google Earth Pro was further used to validate the avulsions by cross-cutting relationships (Fig. S7).

We identified the avulsion site as the location where an avulsion was initiated. The avulsion location remained fixed during the process of the formation of a new channel for the avulsions analyzed here (Supplementary Movie S1). We located the avulsion site and the river mouth just before an avulsion occurred for all identified avulsions and evaluated the avulsion length, L_A , as the streamwise distance between the two locations (Figs. 1, 3A–F, S3). To quantify the temporal evolution of the river mouth and avulsion site, a fixed point was selected at the confluence of Sulengguole River with two anabranches (36°50.011'N, 96°5.518'E; gray asterisk in Fig. 2B). This location is hereafter referred to as the fixed

reference point. Satellite imagery revealed that the fixed reference point remained spatially consistent during the observation period. Distances between the fixed reference point and avulsion sites, and the fixed reference point and river mouth were measured along Sulengguole River course. We computed the streamwise distance of the river mouth from the fixed reference point at least 3 times during each year to quantify the seasonal variability. In addition, we also measured the streamwise distance of the river mouth from the fixed reference point on the satellite image that best captured the avulsion.

Finally, we visualized the distinct deltaic lobes of the Sulengguole River by analyzing the Landsat images during dryer periods of a year when the water level was low after the abandonment of the lobe (Fig. S5). Given the water persistence maps generated from Landsat imagery, we used visual interpretation to draw the boundaries of the individual lobe areas and exported them as shapefile to ArcGIS to generate a map of deltaic lobes.

3.2. Temporal evolution of the North Huoluxun Lake

We quantified the changes in the areal extent of North Huoluxun Lake for the contemporaneous period of observation of lobe-scale avulsions on the Sulengguole River. We used Global Surface Water datasets, which categorized surface water areas into three classes: permanent waters, seasonal waters and ephemeral seasonal surfaces (Pekel et al., 2016). Pekel et al. (2016) defined permanent waters as surfaces that are underwater throughout the year, and seasonal waters are surfaces that are underwater for less than 12 months in a year. We estimated the areal extent of the permanent and seasonal waters by computing the area enclosed within continuous boundaries that demarcate these areas. We manually excluded any sporadic or discrete water bodies, and the surface waters that corresponded to the river water by visual inspection for the computation of the areal extent of the lake. Ephemeral seasonal surfaces are flood event-based areas with moisture, also called wet lands (Li et al., 2018), and are not the focus of this study. All the data were processed through Google Earth Engine and ArcGIS.

3.3. Morphometry of the Sulengguole River

We used the TDX-12 m digital elevation data to estimate reach-scale slope, S , of the Sulengguole River. The TanDEM-X mission was carried out by German AeroSpace Centre and Airbus deployed TerraSAR-X and TerraSAR-X equipped with Synthetic Aperture Radar (SAR) for Digital Elevation Measurement (TanDEM) on a global scale (Wessel et al., 2018; Zink et al., 2014). The mission launched a global, 12-m TanDEM-X product, which covered all land surfaces with a spatial resolution of 0.4 arc seconds (~ 12 m). The absolute vertical accuracy of TDX-12 m could be up to 2 m (Hawker et al., 2019; Wessel et al., 2018; Zink et al., 2014). A recent study demonstrated that TDX-12 m data enabled the characterization of topographic features in the dryland low-gradient, unvegetated Rio Colorado terminus system with accuracy of < 0.5 m (Li et al., 2020). We validated the TDX-12 m data for the Sulengguole River with differential Global Positioning System (dGPS) field surveys (Fig. S9, Table S1). Due to speckle noise, TDX-12 m data were smoothed using a feature preserving filter, which has been previously tested in low-gradient river systems (Li et al., 2020; Lindsay et al., 2019). Longitudinal river profile was extracted from TDX-12 m data, and we evaluated the slope over 7 km windows by fitting a linear regression line between elevation and the streamwise distance (Fig. 2C; Supplementary text).

We used an empirical width-to-depth relationship developed for single-threaded rivers in unvegetated basins to estimate the bankfull flow depth upstream of the avulsion sites (Ielpi and Lapôtre, 2020). To test the validity of this empirical relationship to our field site, we compared the estimated bankfull flow depths from the empirical relationship with field-measured bankfull flow depths at 11 locations along a 2.5 km long reach of the Sulengguole river (Figs. 2C, S10; Supplementary Text). The surveyed reach is located ~ 70 km upstream of the permanent lake boundary (Fig. 2C), which is significantly upstream of the avulsion sites, and hence, could not be directly used to estimate the backwater lengthscale of the Sulengguole river.

4. Results

4.1. Evolution of the Sulengguole River delta

The evolution of the distal Sulengguole River was characterized by river-mouth progradation and construction of delta lobes, which were punctuated by lobe-scale avulsions (Fig. 3; Supplementary Movie S1). We identified six lobe-scale river avulsions on the

Sulengguole River within the observation period (Figs. 3A-F). All observed avulsions were full avulsions, where the parent channel was completely abandoned and the new daughter channel captured all the flow (Fig. 3). We observed the channel relocation for 5 avulsions that were initiated in 1989, 1997, 2003, 2007 and 2008 C.E., which occurred when seasonal waters intruded landward beyond the permanent lake boundary (Fig. 3). We could not locate the time of the oldest avulsion; however, we constrained the occurrence of this avulsion between 1977 C.E. and 1986 C.E. (Fig. S4). We assigned 1982 C.E. as the time of the oldest avulsion—average of the constrained duration for the avulsion.

The six lobe-scale avulsions resulted in the Sulengguole River feeding water and sediment to distinct deltaic lobes (Fig. 3G). The lobe-scale avulsion cycles on the Sulengguole River displayed similar characteristics. The new channel path was typically shorter than the parent channel length before avulsion (Fig. 3), similar to experimental observations of deltaic evolution (Ganti et al., 2016b). Channel abandonment was gradual, typically lasting one to two years when both the old and new channel paths were active (Fig. S6). During the avulsion cycle, we observed river-mouth progradation, river bifurcation, intralobe avulsions, and crevasse splays (Fig. S6). The intralobe avulsions and crevasse splays are also evident as channel cross-cutting relationships within delta lobes on high-resolution satellite imagery (Fig. S7).

We quantified the avulsion length, L_A , for the six avulsions from satellite imagery (Fig. 3A-F). For avulsions that occurred after 1986 C.E., we chose the satellite image that best captured the avulsion (Figs. 3B-F); however, we used the satellite image from 1986 C.E. to evaluate L_A for the oldest lobe-scale avulsion that occurred before 1986 C.E. (Fig. 3A). The avulsion lengths were consistent across the 6 avulsions with a mean and standard deviation of 3.48 km and 1.60 km, respectively. The minimum and maximum avulsion lengths were 1.90 km and 5.91 km, respectively. We did not find a statistically significant temporal trend in the measured avulsion lengths (Fig. S8).

4.2. Landward retreat of river mouth and avulsion sites

Our results indicate that the North Huoluxun Lake expanded during the observation period (Fig. 4). The areal extent of the permanent water was stable during the observation period with a mean of 45.2 km², and maximum and minimum values of 48 km² and 38.2 km², respectively. We did not observe a statistically significant temporal trend in the areal extent of the permanent waters with a rate of change of -0.12 ± 0.19 km²/yr at a 95% confidence level (Fig. 4E). However, the areal extent of the seasonal lake water near the Sulengguole River terminus showed substantial variation (Figs. 3, 4; Supplementary Movie S1). The mean area of the seasonal water was 26.8 km² with maximum and minimum values of 54.2 km² and 0.8 km², respectively. We observed a statistically significant temporal trend in the area of seasonal waters with a rate of change of 1.94 ± 0.68 km²/yr at a 95% confidence level (Fig. 4E). The combined areal extent of the permanent and seasonal waters of the lake also showed a statistically significant temporal trend with a rate of change of 1.82 ± 0.75 km²/yr at a 95% confidence level (Fig. 4E). These results demonstrate that the areal extent of the North Huoluxun Lake increased during the observation period (Fig. 4), likely due to the increase in precipitation extremes or glacial snowmelt (Duan, 2018; Li et al., 2019), which caused the progressive downstream drowning of the river delta.

The increase in the areal extent of the lake waters caused the Sulengguole river mouth to retreat landward (Fig. 3G). The streamwise distance of the river mouth from the fixed reference point revealed both the variability in the river-mouth location caused by the seasonal variation of the lake level, and also the river-mouth progradation over avulsion cycles (Fig. 5A). Avulsions caused river-

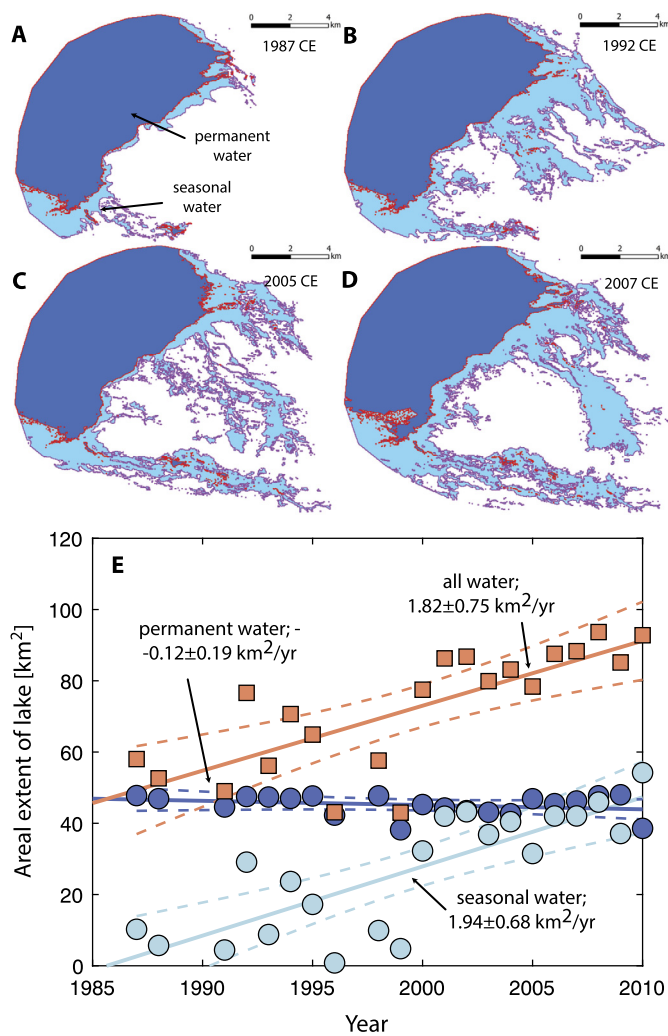


Fig. 4. Expansion of the North Huoluxun Lake. Surface water maps of the permanent waters (dark blue) and seasonal waters (light blue) of the North Huoluxun Lake derived from the Global Surface Water dataset (Pekel et al., 2016) in the year (A) 1987, (B) 1992, (C) 2005, and (D) 2007 C.E. (E) The temporal evolution of the areal extent of the permanent lake waters (royal blue circles), seasonal lake waters (cyan circles), and the combined lake waters (orange squares). The solid and dashed lines indicate the best fit linear trend and their 95% confidence bounds, respectively.

length shortening, which manifested as a sharp decline in the distance of the river mouth from the fixed reference point (Fig. 5A). To quantify the average rate of river-mouth retreat, we measured the distance of the river mouth just before avulsion from the fixed reference point and found that the river mouth retreated upstream by 7.80 km over the 6 avulsion cycles at a rate of 0.31 ± 0.17 km/yr at a 95% confidence level (Fig. 5A).

Results show that the avulsion sites retreated upstream in concert with the river mouth (Figs. 3G, 5A). The avulsion sites retreated upstream by 6.28 km over the 6 avulsion cycles, similar to the river-mouth retreat distance. The average rate of upstream retreat of the avulsion sites is 0.22 ± 0.07 km/yr, consistent with the river-mouth retreat rate (Fig. 5A).

4.3. Backwater scaling of the avulsion length

Results indicate that the avulsion sites were not coincident with a topographic slope-break (Fig. 2C), consistent with lobe-scale avulsions on large, lowland river deltas (Ganti et al., 2014). We computed the backwater lengthscale of the Sulengguole River to test if the measured avulsion lengths, L_A , scaled with the backwater lengthscale (Fig. 1). The estimated channel-bed slope upstream

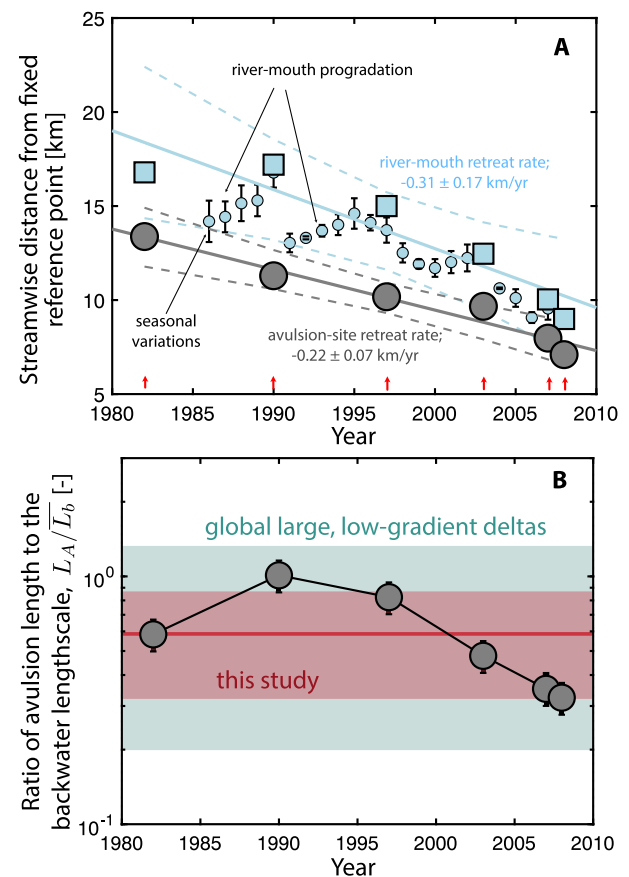


Fig. 5. Temporal evolution of river mouth and avulsion sites. (A) The temporal trend of the landward retreat of the river mouth (blue squares) and avulsion site (gray circles) as measured from the fixed reference point (gray asterisk in Fig. 2B) at the time of avulsion. The solid and dashed lines indicate the best-fitting linear regression line and the 95% confidence bounds, respectively. The small blue circles show the variations in the river mouth location annually, where the river-mouth location was measured at least 3 times during a year. The error bars show the seasonal variations in river-mouth location to the lake-level fluctuations, and the larger trends in the blue circle markers highlight river-mouth progradation and river-length shortening by avulsion (time of avulsions are marked by red arrows). (B) Ratio of the measured avulsion length to the estimated backwater lengthscale for the lobe-scale avulsions on the Sulengguole River. The red shaded area denotes the mean and standard deviation of the dimensionless avulsion length ($L_A/\bar{L}_b = 0.60 \pm 0.27$) for the Sulengguole River. The shaded green area denotes the range of dimensionless avulsion length for a global compilation of large, low-gradient river deltas ($L_A/\bar{L}_b \in [0.2, 1.31]$) (Brooke et al., 2020; Chadwick et al., 2019; Ganti et al., 2019).

of the avulsion sites was $S = 1.75 \times 10^{-4}$ (95% confidence bounds of 1.72×10^{-4} and 1.77×10^{-4}) (Fig. 2C). Results indicated that the empirical width-to-depth scaling of Ielpi and Lapôtre (2020) is applicable to our field site, with the predicted bankfull flow depth and the measured bankfull flow depth showing good agreement at a location that is ~ 70 km upstream of the permanent lake boundary (Fig. S10). Therefore, we applied this empirical relation to estimate the bankfull flow depth upstream of the avulsion site. The bankfull channel width between the fixed reference point and the avulsion sites, estimated using 175 independent measurements from Google Earth Pro imagery, is 15.8 ± 2.7 m (mean and standard deviation), which yielded $h_c = 1.02 \pm 0.26$ m (mean and standard deviation). Together, the estimated S and h_c yielded a backwater lengthscale of $\bar{L}_b = 5.85 \pm 0.86$ km (mean and standard deviation) for the Sulengguole River.

Results demonstrate that L_A scales with \bar{L}_b for all 6 lobe-scale avulsions on the Sulengguole River. The dimensionless avulsion length (Chadwick et al., 2019; Ganti et al., 2019), defined as the ratio of L_A to \bar{L}_b , is $L_A/\bar{L}_b = 0.60 \pm 0.27$ (mean and standard devi-

ation; Fig. 5B). This value is similar to the reported dimensionless avulsion length for large, lowland deltas of $L_A/\bar{L}_b = 0.84 \pm 0.32$ (mean and standard deviation), with a minimum and maximum value of 0.20 and 1.30, respectively (Fig. 5B) (Brooke et al., 2020; Chadwick et al., 2019; Ganti et al., 2019). These results demonstrate that, despite significant river-mouth retreat, avulsions occurred within the backwater zone of the Sulengguole River (Fig. 1B).

Our results also demonstrate that the avulsion sites on the Sulengguole River were not coincident with an abrupt break in the topographic slope of the surrounding floodplain profiles (Fig. S11)—a key prediction under the geometric hypothesis for backwater-scaled avulsions (Ratliff et al., 2021). These results suggest that the difference between in-channel and floodplain sedimentation rates is small in Sulengguole River basin, and the origin of the avulsion sites is likely tied to the morphodynamic feedbacks arising from natural flood-discharge variability.

5. Discussion and conclusions

Our results provide field evidence for how avulsion sites on lowland deltas will respond to the landward retreat of the river mouth. Results demonstrate that river-mouth retreat will necessarily cause the avulsion sites on deltas to translate upstream at a commensurate rate such that the avulsion length will remain constant and scale with the backwater lengthscale (Figs. 5A, 5B). Theory indicates that this landward shift in the avulsion sites should occur because the morphodynamics that lead to preferential sediment accumulation within the backwater zone is fundamentally tied to the river-mouth location (Chadwick et al., 2020; Ganti et al., 2016a). Results also indicate that backwater hydrodynamics play a primary role in setting the location of lobe-scale avulsions on low-gradient rivers draining into lakes (Fig. 5B), similar to low-gradient coastal rivers (Chadwick et al., 2019; Chatanantavet et al., 2012; Ganti et al., 2016a, 2014; Jerolmack, 2009). The future fate of lowland deltas has received considerable attention (Blum and Roberts, 2009; Chadwick et al., 2020; Syvitski et al., 2009; Vörösmarty et al., 2009); however, global lakes are already responding rapidly to environmental stressors (Woolway et al., 2020). Our results indicate that the contraction and expansion of lakes that have occurred in the last five decades (Ma et al., 2010; Woolway et al., 2020) may already have led to the lakeward and landward translation of the historical avulsion sites on deltas formed at the lake margins (Fig. 5).

The results have substantial implications for future flood risk management on large, low-gradient deltas. Theory indicates that large deltas such as the Paraná and the Rhine-Meuse are sediment starved to the point that river-mouth retreat and land loss are inevitable under historical rates of relative sea-level rise (Chadwick et al., 2020). While other major deltas such as the Mississippi, Amazon, Orinoco, and Nile have kept pace with the relative sea-level rise through the Holocene, they are also likely to experience river-mouth retreat with storm surges and the ongoing and projected acceleration in the relative sea-level rise rates (Chadwick et al., 2020; Edmonds et al., 2020). The extremely low slopes that characterize large river deltas make them especially vulnerable to flooding, with $>100,000$ km² of deltaic land less than 2 m above mean sea level (Syvitski et al., 2009). Thus, even a small magnitude rise in relative sea level and storm surges on sediment-starved deltas can potentially cause kilometer-scale river-mouth retreat. Our results indicate that river-mouth retreat on these large deltas can cause avulsion sites to migrate inland by tens to hundreds of kilometers, given consistent supply of water and sediment that control the backwater lengthscale (Fig. 5). For example, the Old River Control Structure prevents the avulsion of the Mississippi River into the Atchafalaya River at the historical avulsion site; how-

ever, our results indicate that river-mouth retreat will create a new preferential location for lobe-scale avulsions upstream (Fig. 5), rendering the existing engineering structure ineffective. Our results also bolster the notion that the backwater lengthscale is a reliable, first-order predictor of future lobe-scale avulsions on deltas (Fig. 5B), which could inform management actions for flood mitigation.

The results add to the growing recognition that climate change and human activities will make avulsions a serious and frequent future flood hazard on deltas (Brooke et al., 2020; Chadwick et al., 2020). Changes in frequency and magnitude of flood extremes—an expected consequence of climate change (Hirabayashi et al., 2013)—and the fining of fluvial sediment supply by the trapping of coarse sediment behind dams are expected to cause the avulsion sites on lowland deltas to occur further upstream of the backwater zone (Brooke et al., 2020). Our results indicate that the reduction in sediment supply, acceleration of sea-level rise rates and storm surges will exacerbate this flooding risk because avulsion sites will translate further inland with river-mouth retreat (Fig. 5B), affecting upstream communities that have historically seldom experienced avulsion-induced flood hazards.

Our results also have implications for paleoenvironmental interpretation of fluvial deposits on Mars. Multiple stacked depositional lobes with spatially distributed avulsion sites are a diagnostic feature of rivers draining into lakes and seas (Figs. 3G, 5), which is in contrast to lobe-scale avulsions on alluvial fans that are tied to abrupt topographic changes (Ganti et al., 2014). These results suggest that spatially distributed avulsion sites can serve as a tool to distinguish fan deposits from delta deposits, thus, enabling the interpretation of paleolakes and seas on Mars and other planetary bodies (Adler et al., 2019; DiBiase et al., 2013).

Ultimately, results suggest that the drowning of river deltas from accelerated relative sea-level rise and coastal inundation will result in the upstream translation of the historical avulsion sites. This phenomenon will expose new inland communities to the risks of catastrophic flooding, and the manner in which the avulsion sites will migrate inland is predictable and consistent with the backwater hypothesis for lobe-scale avulsions on deltas.

CRedit authorship contribution statement

Jianguang Li: Conceptualization, Investigation, Methodology, Supervision, Visualization, Writing – original draft, Writing – review & editing. **Vamsi Ganti:** Conceptualization, Investigation, Methodology, Supervision, Visualization, Writing – original draft, Writing – review & editing. **Chenglong Li:** Investigation, Methodology. **Hao Wei:** Investigation, Methodology.

Declaration of competing interest

The authors declare that they have no known competing financial interests or personal relationships that could have appeared to influence the work reported in this paper.

Data availability

USGS/NASA Landsat satellite imagery is freely available from the USGS Earth Explorer (<https://earthexplorer.usgs.gov/>). Surface water masks are available from the JRC Global Surface Water 1984–2018 data sets (<https://global-surface-water.appspot.com/>) (Pekel et al., 2016). Global compilation of avulsion lengths on low-gradient deltas were previously published (Chatanantavet et al., 2012; Ganti et al., 2019, 2014; Jerolmack and Mohrig, 2007; Jerolmack and Swenson, 2007; Moodie et al., 2019), and compiled in (Brooke et al., 2020). All other data needed to evaluate the conclusions in the paper are present in the paper and/or Supplementary information files.

Acknowledgements

This research was supported by the National Natural Science Foundation of China (No. 41972114, No. 42172133, No. 41602121), Wuhan Applied Foundational Frontier Project (No. 2020020601012281), and the Fundamental Research Funds for the Central Universities, China University of Geosciences, Wuhan (No. CUG150616) to J. Li and by the National Science Foundation EAR 1935669 grant to Ganti. J. Li thanks the German Aerospace Center for the TanDEM-X data (Grant No. GEOL2302).

Appendix A. Supplementary material

Supplementary material related to this article can be found online at <https://doi.org/10.1016/j.epsl.2021.117270>.

References

- Adler, J.B., Bell III, J.F., Fawdon, P., Davis, J., Warner, N.H., Sefton-Nash, E., Harrison, T.N., 2019. Hypotheses for the origin of the Hypanis fan-shaped deposit at the edge of the Chryse escarpment, Mars: is it a delta? *Icarus* 319, 885–908. <https://doi.org/10.1016/j.icarus.2018.05.021>.
- Adrian, R., O'Reilly, C.M., Zagarese, H., Baines, S.B., Hessen, D.O., Keller, W., Livingstone, D.M., Sommaruga, R., Straille, D., Van Donk, E., Wehnenmeyer, G.A., Winder, M., 2009. Lakes as sentinels of climate change. *Limnol. Oceanogr.* 54, 2283–2297. https://doi.org/10.4319/lo.2009.54.6_part_2.2283.
- Best, J., Darby, S.E., 2020. The pace of human-induced change in large rivers: stresses, resilience, and vulnerability to extreme events. *One Earth* 2, 510–514.
- Blum, M.D., Roberts, H.H., 2009. Drowning of the Mississippi Delta due to insufficient sediment supply and global sea-level rise. *Nat. Geosci.* 2, 488–491. <https://doi.org/10.1038/ngeo553>.
- Brooke, S.A.S., Ganti, V., Chadwick, A.J., Lamb, M.P., 2020. Flood variability determines the location of lobe-scale avulsions on deltas: Madagascar. *Geophys. Res. Lett.* 47, e2020GL088797. <https://doi.org/10.1029/2020GL088797>.
- Chadwick, A.J., Lamb, M.P., Ganti, V., 2020. Accelerated river avulsion frequency on lowland deltas due to sea-level rise. *Proc. Natl. Acad. Sci.* 117, 17584–17590. <https://doi.org/10.1073/pnas.1912351117>.
- Chadwick, A.J., Lamb, M.P., Moodie, A.J., Parker, G., Nittrouer, J.A., 2019. Origin of a preferential avulsion node on lowland river deltas. *Geophys. Res. Lett.* 46, 4267–4277. <https://doi.org/10.1029/2019GL082491>.
- Chatanantavet, P., Lamb, M.P., 2014. Sediment transport and topographic evolution of a coupled river and river plume system: an experimental and numerical study. *J. Geophys. Res., Earth Surf.* 119, 1263–1282. <https://doi.org/10.1002/2013JF002810>.
- Chatanantavet, P., Lamb, M.P., Nittrouer, J.A., 2012. Backwater controls of avulsion location on deltas. *Geophys. Res. Lett.* 39. <https://doi.org/10.1029/2011GL050197>.
- DiBiase, R.A., Limaye, A.B., Scheingross, J.S., Fischer, W.W., Lamb, M.P., 2013. Deltaic deposits at Aeolis Dorsa: sedimentary evidence for a standing body of water on the northern plains of Mars. *J. Geophys. Res., Planets* 118, 1285–1302. <https://doi.org/10.1002/jgre.20100>.
- Duan, S., 2018. Lake evolution in the Qaidam Basin during 1976–2015 and their changes in response to climate and anthropogenic factors. *J. Lake Sci.* 30, 256–265. <https://doi.org/10.18307/2018.0125>.
- Edmonds, D.A., Caldwell, R.L., Brondizio, E.S., Siani, S.M.O., 2020. Coastal flooding will disproportionately impact people on river deltas. *Nat. Commun.* 11, 4741. <https://doi.org/10.1038/s41467-020-18531-4>.
- Erban, L.E., Gorelick, S.M., Zebker, H.A., 2014. Groundwater extraction, land subsidence, and sea-level rise in the Mekong Delta, Vietnam. *Environ. Res. Lett.* 9, 84010. <https://doi.org/10.1088/1748-9326/9/8/084010>.
- Ganti, V., Chadwick, A.J., Hassenruck-Gudipati, H.J., Fuller, B.M., Lamb, M.P., 2016a. Experimental river delta size set by multiple floods and backwater hydrodynamics. *Sci. Adv.* 2. <https://doi.org/10.1126/sciadv.1501768>.
- Ganti, V., Chadwick, A.J., Hassenruck-Gudipati, H.J., Lamb, M.P., 2016b. Avulsion cycles and their stratigraphic signature on an experimental backwater-controlled delta. *J. Geophys. Res., Earth Surf.* 121, 1651–1675. <https://doi.org/10.1002/2016JF003915>.
- Ganti, V., Chu, Z., Lamb, M.P., Nittrouer, J.A., Parker, G., 2014. Testing morphodynamic controls on the location and frequency of river avulsions on fans versus deltas: Huanghe (Yellow River), China. *Geophys. Res. Lett.* 41, 7882–7890. <https://doi.org/10.1002/2014GL061918>.
- Ganti, V., Lamb, M.P., Chadwick, A.J., 2019. Autogenic erosional surfaces in fluvio-deltaic stratigraphy from floods, avulsions, and backwater hydrodynamics. *J. Sediment. Res.* 89, 815–832. <https://doi.org/10.2110/jsr.2019.40>.
- Giosan, L., Syvitski, J., Constantinescu, S., Day, J., 2014. Climate change: protect the world's deltas. *Nat. News* 516, 31.
- Hawker, L., Neal, J., Bates, P., 2019. Accuracy assessment of the TanDEM-X 90 Digital Elevation Model for selected floodplain sites. *Remote Sens. Environ.* 232, 111319. <https://doi.org/10.1016/j.rse.2019.111319>.
- Higgins, S., Overeem, I., Tanaka, A., Syvitski, J.P.M., 2013. Land subsidence at aquaculture facilities in the Yellow River Delta, China. *Geophys. Res. Lett.* 40, 3898–3902. <https://doi.org/10.1002/grl.50758>.
- Hirabayashi, Y., Mahendran, R., Koirala, S., Konoshima, L., Yamazaki, D., Watanabe, S., Kim, H., Kanae, S., 2013. Global flood risk under climate change. *Nat. Clim. Change* 3, 816–821. <https://doi.org/10.1038/nclimate1911>.
- Ielpi, A., Lapôtre, M.G.A., 2020. A tenfold slowdown in river meander migration driven by plant life. *Nat. Geosci.* 13, 82–86. <https://doi.org/10.1038/s41561-019-0491-7>.
- Jerolmack, D.J., 2009. Conceptual framework for assessing the response of delta channel networks to Holocene sea level rise. *Quat. Sci. Rev.* 28, 1786–1800. <https://doi.org/10.1016/j.quascirev.2009.02.015>.
- Jerolmack, D.J., Mohrig, D., 2007. Conditions for branching in depositional rivers. *Geology* 35, 463–466. <https://doi.org/10.1130/G23308A.1>.
- Jerolmack, D.J., Swenson, J.B., 2007. Scaling relationships and evolution of distributary networks on wave-influenced deltas. *Geophys. Res. Lett.* 34. <https://doi.org/10.1029/2007GL031823>.
- Kidder, T.R., Liu, H., 2017. Bridging theoretical gaps in geoarchaeology: archaeology, geoarchaeology, and history in the Yellow River valley, China. *Archaeol. Anthropol. Sci.* 9, 1585–1602. <https://doi.org/10.1007/s12520-014-0184-5>.
- Kim, W., Mohrig, D., Twilley, R., Paola, C., Parker, G., 2009. Is it feasible to build new land in the Mississippi River Delta? *Eos Trans. AGU* 90, 373–374. <https://doi.org/10.1029/2009EO420001>.
- Lamb, M.P., Nittrouer, J.A., Mohrig, D., Shaw, J., 2012. Backwater and river plume controls on scour upstream of river mouths: implications for fluvio-deltaic morphodynamics. *J. Geophys. Res., Earth Surf.* 117. <https://doi.org/10.1029/2011JF002079>.
- Levermann, A., Clark, P.U., Marzeion, B., Milne, G.A., Pollard, D., Radic, V., Robinson, A., 2013. The multimillennial sea-level commitment of global warming. *Proc. Natl. Acad. Sci.* 110, 13745–13750. <https://doi.org/10.1073/pnas.1219414110>.
- Li, H., Mao, D., Li, X., Wang, Z., Wang, C., 2019. Monitoring 40-year lake area changes of the Qaidam Basin, Tibetan Plateau, using landsat time series. *Remote Sens.* 11, 343. <https://doi.org/10.3390/rs11030343>.
- Li, J., Yang, X., Maffei, C., Tooth, S., Yao, G., 2018. Applying independent component analysis on sentinel-2 imagery to characterize geomorphological responses to an extreme flood event near the non-vegetated Río Colorado Terminus, Salar de Uyuni, Bolivia. *Remote Sens.* 10, 725. <https://doi.org/10.3390/rs10050725>.
- Li, J., Zhao, Y., Bates, P., Neal, J., Tooth, S., Hawker, L., Maffei, C., 2020. Digital Elevation Models for topographic characterisation and flood flow modelling along low-gradient, terminal dryland rivers: a comparison of spaceborne datasets for the Río Colorado, Bolivia. *J. Hydrol.* 591, 125617. <https://doi.org/10.1016/j.jhydrol.2020.125617>.
- Lindsay, J.B., Francioni, A., Cockburn, J.M.H., 2019. LiDAR DEM smoothing and the preservation of drainage features. *Remote Sens.* <https://doi.org/10.3390/rs11161926>.
- Ma, R., Duan, H., Hu, C., Feng, X., Li, A., Ju, W., Jiang, J., Yang, G., 2010. A half-century of changes in China's lakes: global warming or human influence? *Geophys. Res. Lett.* 37. <https://doi.org/10.1029/2010GL045514>.
- Meehl, G.A., Washington, W.M., Collins, W.D., Arblaster, J.M., Hu, A., Buja, L.E., Strand, W.C., Teng, H., 2005. How much more global warming and sea level rise? *Science* 307, 1769–1772. <https://doi.org/10.1126/science.1106663>.
- Mohrig, D., Heller, P.L., Lyons, W.J., 2000. Interpreting avulsion process from ancient alluvial sequences: Guadalupe-Matarranya system (northern Spain) and Wasatch Formation (western Colorado). *Geol. Soc. Am. Bull.* 112, 1787–1803. [https://doi.org/10.1130/0016-7606\(2000\)112<1787:IAPFAA>2.0.CO;2](https://doi.org/10.1130/0016-7606(2000)112<1787:IAPFAA>2.0.CO;2).
- Moodie, A.J., Nittrouer, J.A., Ma, H., Carlson, B.N., Chadwick, A.J., Lamb, M.P., Parker, G., 2019. Modeling deltaic lobe-building cycles and channel avulsions for the Yellow River Delta, China. *J. Geophys. Res., Earth Surf.* 124, 2438–2462. <https://doi.org/10.1029/2019JF005220>.
- Nicholls, R.J., 2004. Coastal flooding and wetland loss in the 21st century: changes under the SRES climate and socio-economic scenarios. *Glob. Environ. Change* 14, 69–86. <https://doi.org/10.1016/j.gloenvcha.2003.10.007>.
- Nicholls, R.J., Cazenave, A., 2010. Sea-level rise and its impact on coastal zones. *Science* 328, 1517–1520. <https://doi.org/10.1126/science.1185782>.
- Otsu, N., 1979. A threshold selection method from gray-level histograms. *IEEE Trans. Syst. Man Cybern.* 9, 62–66. <https://doi.org/10.1109/TSMC.1979.4310076>.
- Paola, C., Mohrig, D., 1996. Palaeohydraulics revisited: palaeoslope estimation in coarse-grained braided rivers. *Basin Res.* 8, 243–254. <https://doi.org/10.1046/j.1365-2117.1996.00253.x>.
- Pekel, J.-F., Cottam, A., Gorelick, N., Belward, A.S., 2016. High-resolution mapping of global surface water and its long-term changes. *Nature* 540, 418–422. <https://doi.org/10.1038/nature20584>.
- Ratliff, K.M., Hutton, E.W.H., Murray, A.B., 2021. Modeling long-term delta dynamics reveals persistent geometric river avulsion locations. *Earth Planet. Sci. Lett.* 559, 116786. <https://doi.org/10.1016/j.epsl.2021.116786>.
- Slingerland, R., Smith, N.D., 2004. River avulsions and their deposits. *Annu. Rev. Earth Planet. Sci.* 32, 257–285. <https://doi.org/10.1146/annurev.earth.32.101802.120201>.

- Syvitski, J.P.M., 2008. Deltas at risk. *Sustain. Sci.* 3, 23–32.
- Syvitski, J.P.M., Kettner, A.J., Overeem, I., Hutton, E.W.H., Hannon, M.T., Brakenridge, G.R., Day, J., Vörösmarty, C., Saito, Y., Giosan, L., Nicholls, R.J., 2009. Sinking deltas due to human activities. *Nat. Geosci.* 2, 681–686. <https://doi.org/10.1038/ngeo629>.
- Syvitski, J.P.M., Vörösmarty, C.J., Kettner, A.J., Green, P., 2005. Impact of humans on the flux of terrestrial sediment to the global coastal ocean. *Science* 308, 376–380. <https://doi.org/10.1126/science.1109454>.
- Vörösmarty, C.J., Meybeck, M., Fekete, B., Sharma, K., Green, P., Syvitski, J.P.M., 2003. Anthropogenic sediment retention: major global impact from registered river impoundments. *Glob. Planet. Change* 39, 169–190. [https://doi.org/10.1016/S0921-8181\(03\)00023-7](https://doi.org/10.1016/S0921-8181(03)00023-7).
- Vörösmarty, C.J., Syvitski, J., John, D.A.Y., De Sherbinin, A., Giosan, L., Paola, C., 2009. Battling to save the world's river deltas. *Bull. At. Sci.* 65, 31–43. <https://doi.org/10.2968/065002005>.
- Wang, S., Toumi, R., 2021. Recent migration of tropical cyclones toward coasts. *Science* 371, 514–517. <https://doi.org/10.1126/science.abb9038>.
- Wessel, B., Huber, M., Wohlfart, C., Marschalk, U., Kosmann, D., Roth, A., 2018. Accuracy assessment of the global TanDEM-X Digital Elevation Model with GPS data. *ISPRS J. Photogramm. Remote Sens.* 139, 171–182. <https://doi.org/10.1016/j.isprsjprs.2018.02.017>.
- Woodruff, J.D., Irish, J.L., Camargo, S.J., 2013. Coastal flooding by tropical cyclones and sea-level rise. *Nature* 504, 44–52. <https://doi.org/10.1038/nature12855>.
- Woolway, R.I., Kraemer, B.M., Lenters, J.D., Merchant, C.J., O'Reilly, C.M., Sharma, S., 2020. Global lake responses to climate change. *Nat. Rev. Earth Environ.* 1, 388–403. <https://doi.org/10.1038/s43017-020-0067-5>.
- Xu, H., 2006. Modification of normalised difference water index (NDWI) to enhance open water features in remotely sensed imagery. *Int. J. Remote Sens.* 27, 3025–3033. <https://doi.org/10.1080/01431160600589179>.
- Zink, M., Bachmann, M., Brautigam, B., Fritz, T., Hajnsek, I., Moreira, A., Wessel, B., Krieger, G., 2014. TanDEM-X: the new global DEM takes shape. *IEEE Geosci. Remote Sens. Mag.* 2, 8–23. <https://doi.org/10.1109/MGRS.2014.2318895>.